Reliability of dynamically-embedded anchors in soft clay

Joe G. Tom[1], Conleth O'Loughlin[2] and David J. White[3]

1: Geotechnical Engineer
Shell International Exploration and Production Inc.
Houston, TX, 77079
United States of America

2: Professor
Centre for Offshore Foundation Systems
Oceans Graduate School
The University of Western Australia
Crawley WA 6009
Australia

3: Professor of Infrastructure Geotechnics
University of Southampton
Southampton, SO17 1BJ
United Kingdom

Words: 6428

Figures: 13

Tables: 3

Keywords: anchors, floating structures, reliability

ABSTRACT

Floating offshore infrastructure requires geotechnical anchorage for station-keeping. Dynamically embedded anchors are anchors that free-fall through the water column and embed in the seafloor through kinetic energy at impact, enabling efficient installation into soft seabeds. Dynamic installation of plate anchors is an alternative to static embedment methods, such as suction-embedded plate anchors. This paper uses a numerical installation and capacity methodology to explore the factors that control dynamically-embedded plate anchor (DEPLA) capacity and to compare DEPLA reliability with that of statically-embedded plate anchors for two sets of seafloor properties that represent different types of geotechnical uncertainty. Probabilistic Monte Carlo simulations are presented for the two representative conditions using the distribution of the tension loads for an example catenary-moored system. The results quantify the smaller influence of soil strength uncertainty on DEPLAs compared to statically-embedded plates. The smaller influence arises due to dynamically-embedded anchors reaching a deeper embedment in softer soil, counteracting the lower strength. This leads to increased reliability compared to statically-embedded equivalent anchors installed to a specified depth. We quantify the reduction in safety factor that could be used for dynamically-embedded anchor design to achieve similar levels of reliability compared to statically-installed anchors of the same size.

1 Introduction

Floating offshore facilities and vessels are kept on station using mooring systems connected to seabed anchors. Although 'on-bottom' gravity anchors have been used (e.g. Erbich & Neubecker, 1999), the majority of anchors are embedded in the seafloor, either by dragging, driving (e.g., Boylan et al., 2017) or via suction installation (e.g. Andersen et al. 2005). Dynamically-embedded anchors are a potential alternative to these methods with reduced installation time and costs. Dynamic installation is conducted by (i) releasing the anchor from a height above the seabed, (ii) free-fall through the water column and (iii) penetration into the seabed.

Various dynamically-embedded anchors have been developed (Figure 1) that have common analogies to statically-embedded types. For instance, torpedo piles developed by Petrobras (dos Santos et al., 2004) can be viewed as the dynamically-embedded equivalent to driven piles or suction caissons, whereas the Dynamically Embedded Plate Anchor (DEPLA – O'Loughlin et al., 2013a) is equivalent to a suction embedded plate anchor (SEPLA – Wilde et al., 2001). There is significant potential economic and project scheduling benefits for dynamic embedment because each anchor can be installed in less time and smaller vessels with less complex equipment can be utilised (O'Loughlin et al. 2015). However, dynamically-embedded anchors are perceived to have increased risk and uncertainty in installed depth. In contrast, for statically-installed anchors, installation depths are specified by design and confirmed on installation. The depth uncertainty introduced by dynamic installation is the primary concern of this paper.

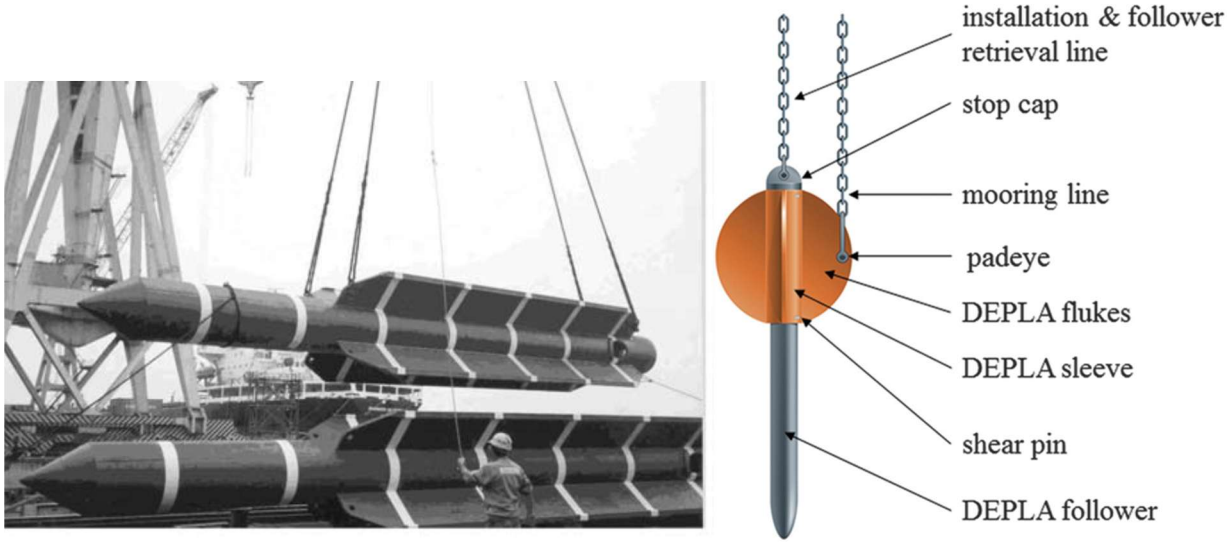

Figure 1. Two dynamically embedded anchor types: dynamically-embedded torpedo pile (left – dos Santos et al., 2004); dynamically-embedded plate anchor (right – Blake and O'Loughlin, 2015).

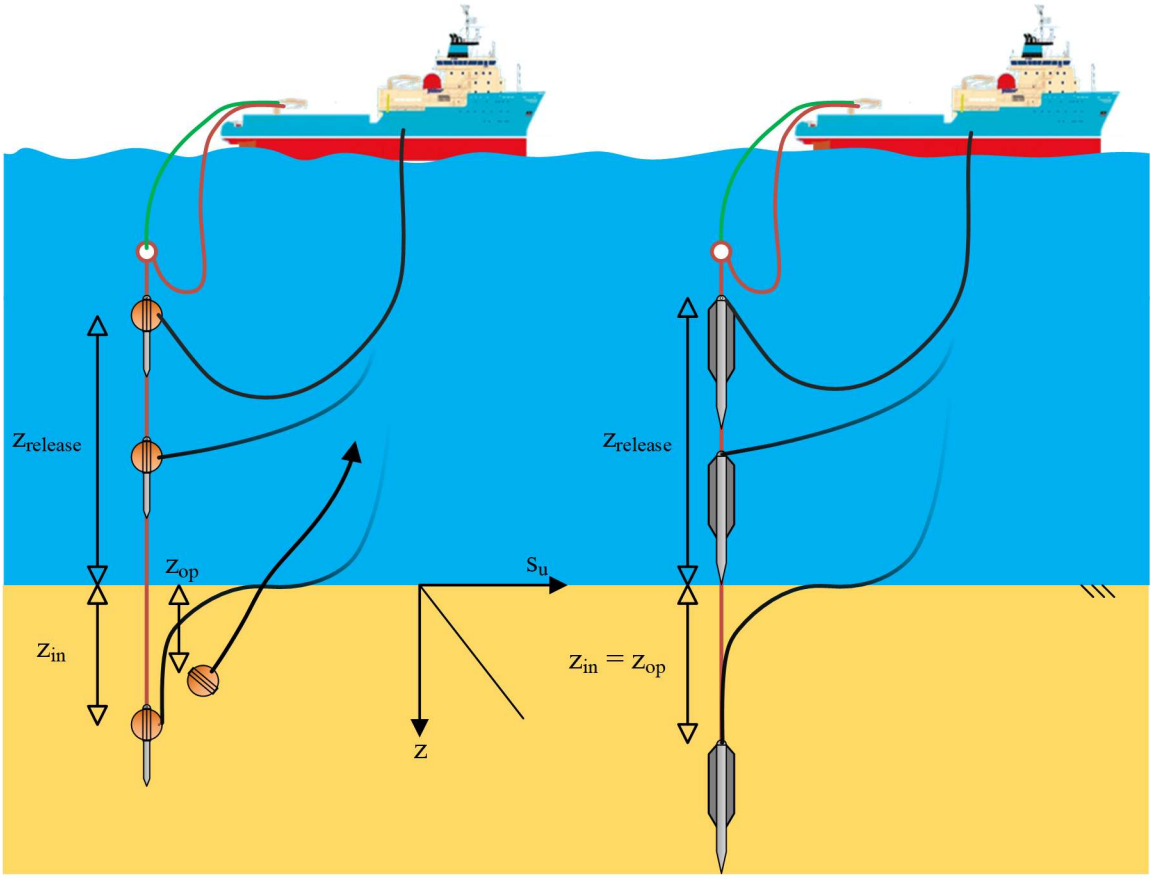

Figure 2. Dynamic installation of a: (a) plate anchor and (b) pile.

Two primary anchoring concepts utilising dynamic installation have been explored in research and implemented on some projects – dynamically-embedded plate anchors (O'Loughlin et al. 2014) and dynamically-embedded piles (e.g. Lieng et al. 1999; dos Santos et al. 2004; Zimmerman et al. 2009) – as illustrated on Figure 2. A dynamically embedded pile is typically a cylindrical object with stabilising fins. The entire object remains in the seabed to serve as the anchor. Holding capacity develops from combinations of self-weight, frictional along the shaft and end bearing, depending on the load inclination at the padeye attachment point. Torpedo piles have been utilised, particularly in Brazil, for both temporary and permanent mooring (Henriques et al. 2010), with a variation used in the Gulf of Mexico for temporary moorings (Zimmerman et al. 2009). Although the ease and economics of installation are attractive, they have a relatively low efficiency, expressed as the ratio of capacity to self-weight (O'Loughlin et al. 2017).

The DEPLA is a plate that is dynamically embedded by penetration of a free-falling dart-shaped object. The central 'follower' of the dart is removed, leaving the flukes embedded in the seabed (Figure 2a). The DEPLA capacity in fine-grained materials, which are undrained during operational loading, derives from plate flow-around failure. The DEPLA provides a higher capacity to installed weight ratio than a similar-sized dynamically-embedded pile due to: (i) the capacity is derived from bearing not friction, and (ii) the follower is removed and reused (O'Loughlin et al. 2017). Although the components contributing to capacity differ between these anchors, the force components that act on the anchors during installation and control the embedment depth are similar.

For both dynamically-embedded anchors, there is uncertainty regarding the installation depth and capacity. The seabed undrained strength plays an important role in this uncertainty, as it controls the resistance bringing the anchor to rest and controls the capacity during loading. However, analyses by O'Loughlin et al. (2017) suggest that uncertainty in seabed strength may actually result in higher relative reliability for a dynamically-embedded anchor because of a self-correcting characteristic – if the soil is weaker than expected the anchor will embed deeper counteracting losses in capacity due to the lower strength, and vice versa. This was also illustrated by O'Loughlin et al. (2016) where DEPLA anchors at two clay sites with strength gradients differing by a factor of 3 showed significantly different embedment but approximately equal capacities.

This paper aims to answer two related questions: (1) do dynamically-embedded anchors have a self-correcting characteristic with respect to variability in seabed properties; and (2) how does the reliability of dynamically-embedded anchors compare with more conventional anchors statically installed to a predetermined depth? To address these questions, we compare the response of a DEPLA with a statically-embedded plate anchor of the same size in soft clay. Dynamic installation is simulated using the anchor embedment model described by O'Beirne et al. (2017a). We first explore the effect of input parameters on anchor performance and how these affect design. Second, we compare the reliability associated with DEPLAs as a permanent mooring solution compared with statically-embedded anchors using Monte Carlo analyses.

2 Dynamic installation analysis: the release-to-rest model

The installation model utilised here was originally described by O'Beirne et al. (2017a), where the governing equation of motion during installation is:

$$F_{net} = (m + m')\frac{d^2z}{dt^2} = W_s - F_b - F_g - F_d \quad (1)$$

where m is the anchor mass, m' is the added mass of water and soil accelerated with the anchor, z is the vertical position of the anchor tip relative to the seabed, t is time, W_s is the submerged weight of the anchor in water, F_b is a buoyancy term associated with the displaced volume of soil, F_g is the seabed geotechnical resistance and F_d represents components of drag resistance acting on the anchor itself, the trailing mooring line and the follower recovery line. These terms are illustrated schematically in Figure 3 for a representative DEPLA.

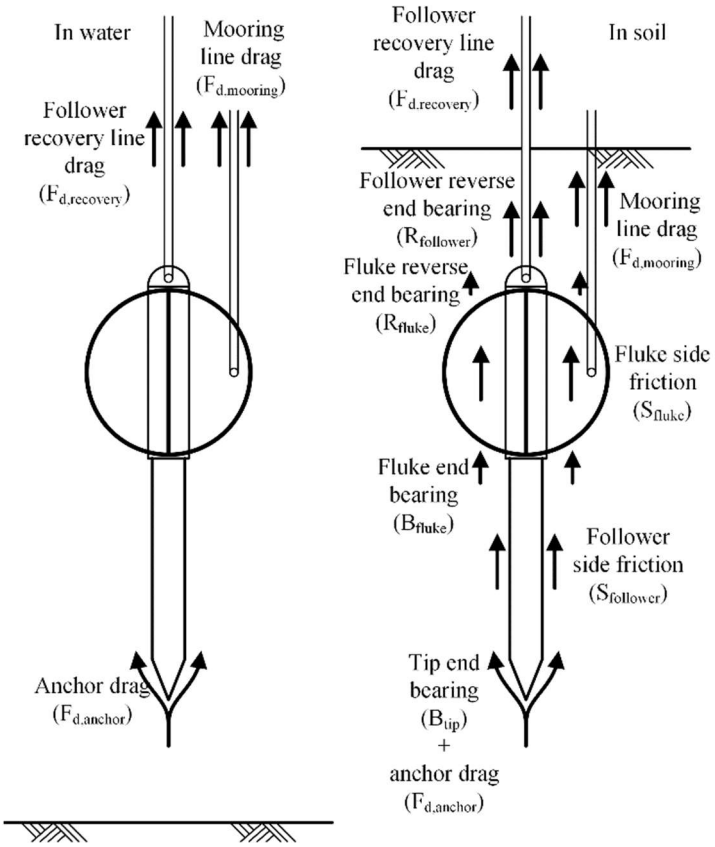

(a)

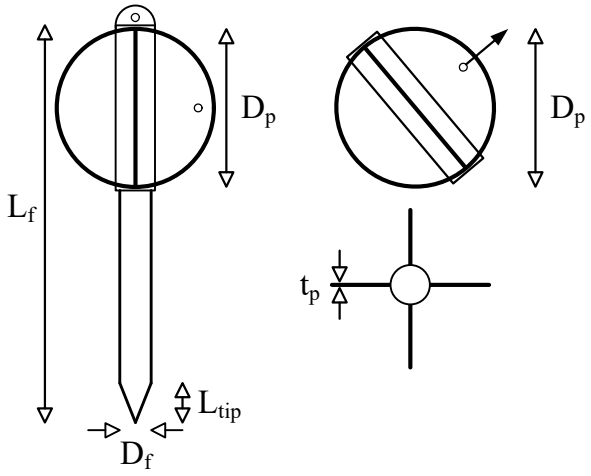

(b)

Figure 3. DEPLA: (a) contributing components of resistance during the installation process; (b) DEPLA dimensions.

The geotechnical resistance on the anchor during penetration (F_g) corresponds to (a) end bearing resistance acting on the anchor tip and projected area of the fluke bottoms, (b) frictional resistance along the anchor shaft and fluke faces and (c) reverse end bearing resistance acting behind the follower and above the flukes:

$$F_g = B_{tip} + B_{fluke} + S_{shaft} + S_{fluke} + R_{follower} + R_{fluke} \quad (2)$$

where B_{tip} and B_{fluke} are the tip and fluke end bearing components, S_{shaft} and S_{fluke} are the side friction developed along the follower shaft and fluke sides, and $R_{follower}$ and R_{fluke} are reverse end bearing components.

The adopted bearing capacity factors are listed in Table 1, as originally proposed by O'Loughlin et al. (2004). These factors have been shown match well with available centrifuge and field data (O'Loughlin et al. 2013, O'Beirne et al. 2017a, 2017b) when applied to the intact (rate-enhanced) undrained strength. The frictional resistance component is equal to the remoulded (rate-enhanced) undrained strength, implying $\alpha \approx 1/S_t$, as commonly assumed for penetration of piles and caissons (e.g. Andersen et al. 2005). During anchor installation, it is assumed that soil closes over the rear of the anchor follower and flukes, such that no cavity forms and reverse end bearing resistance develops at the top of the follower and flukes. O'Loughlin et al. (2013) showed that these components approximately compensate for each other, such that there is minimal net effect on the calculated embedment depth when either assumption is adopted.

The geometry of the anchor is simplified into a structure composed of a conical tip, a cylindrical shaft of constant diameter and two perpendicular circular fluke sections. For simplicity, the top cap where the retrieval line connects to the follower is ignored as it contributes negligible resistance. The tops of the flukes are assumed to terminate at the top of the follower. The parameters L_{tip}, L_f, D_f, D_p and t_p are the length of the anchor tip, the length and diameter of the follower and the diameter and thickness of the plate (fluke) – Figure 3b. Additional parameters relating to installation are the release height, as-installed embedment depth and the keyed embedment during operation: $z_{release}$, z_{in} and z_{op}, respectively (Figure 2a). The trailing line diameter, D_l, affects the drag resistance during free-fall. The non-dimensional ratios of these parameters are presented in Table 1.

The drag that acts on the anchor and following lines during free-fall through the water column

is based on fluid drag coefficients from O'Beirne et al. (2017a), listed in Table 1, which provide good agreement with installation records from field testing of reduced scale anchors. These coefficients could be modified for specific geometries either through reduced scale experiments (e.g. Blake and O'Loughlin, 2015) or computational fluid dynamic analyses (e.g. Raaj et al. 2022) but are taken as constants in the current work. Hence, the drag coefficient acting on the follower recovery and mooring lines is assumed here to not vary with Reynolds number, Re, or length of wetted area (Ackroyd 1982). As discussed in Blake and O'Loughlin (2015), this is appropriate when anchor velocity and hence Re is high, as is the case for the simulations reported later in the paper that consider anchor impact velocities that are 90% of the terminal velocity.

Table 1. Anchor geometry and non-dimensional model parameters.

Property	Follower Length $\frac{L_f}{D_f}$	Follower Tip Length $\frac{L_{tip}}{D_f}$	Plate Diameter $\frac{D_p}{L_f}$	Plate Thickness $\frac{t_p}{D_p}$	Line Diameter $\frac{D_l}{D_f}$	Padeye Eccentricity $\frac{e}{D_p}$	Anchor Tip Bearing Factor $N_{c,tip}$	Fluke Bearing Factor $N_{c,fluke}$	Anchor Drag Coef. $C_{d,anchor}$	Line Drag Coef. $C_{d,line}$
General[1]	12	1.25	0.4	0.05	0.1725	0.45	12	7.5	0.7	0.008[3]
O'Beirne et al. (2017a) Comparison[2]	12.5	1.9	0.4	0.034	0.067	N/A	12	7.5	0.67	0.008, 0.019[3]

Note: (1) Used for sensitivity study and Monte Carlo analysis
(2) Used for validation case. Assume D_f = 0.06 m.
(3) O'Beirne et al. (2017a) used 0.019 for the tests at Erne and 0.008 for larger scale tests at Troll. See O'Bierne et al. (2017a) for details.

This paper assumes soil properties corresponding to a single soil layer with a mudline strength intercept, s_{u0}, a strength gradient with depth, k, and a sensitivity, S_t, representing the ratio of intact to fully remoulded strength. Strain rate effects act to increase the strength (intact or remoulded) following the power law relationship by Biscontin and Pestana (2001):

$$s_u = s_{u,ref}\left(\frac{\dot{\gamma}}{\dot{\gamma}_{ref}}\right)^{\beta} \quad (2)$$

where $\dot{\gamma}$ is the operative soil strain rate, $s_{u,ref}$ is a reference undrained strength measured at a particular reference strain rate, $\dot{\gamma}_{ref}$, for instance corresponding to the strain rate of a laboratory or in situ test. The exponent β controls the increase in undrained strength with strain rate. Although

the shear strain rate during dynamic penetration varies locally around the anchor, it is common practice (e.g. O'Loughlin et al. 2016) to assume an operational strain rate that is proportional to the ratio of the anchor velocity to diameter, v/D_f, so Eq. (2) can be rewritten as:

$$s_u = s_{u,ref}\left(\frac{v/D_f}{(v/D)_{ref}}\right)^{\beta} \tag{3}$$

where $(v/D)_{ref}$ is a reference velocity to diameter ratio at which the reference soil strength, $s_{u,ref}$, applies. This strength is generally found from in situ penetrometer testing (e.g. cone, T-bar or ball penetrometer testing), at penetration velocity, v, with a device of diameter, D.

The installation model has been implemented into Python with a first-order Euler numerical scheme to solve the governing differential equation. Figure 4 shows a validation example based on results from trial anchor installations in the North Sea (described by O'Beirne et al. 2017a).

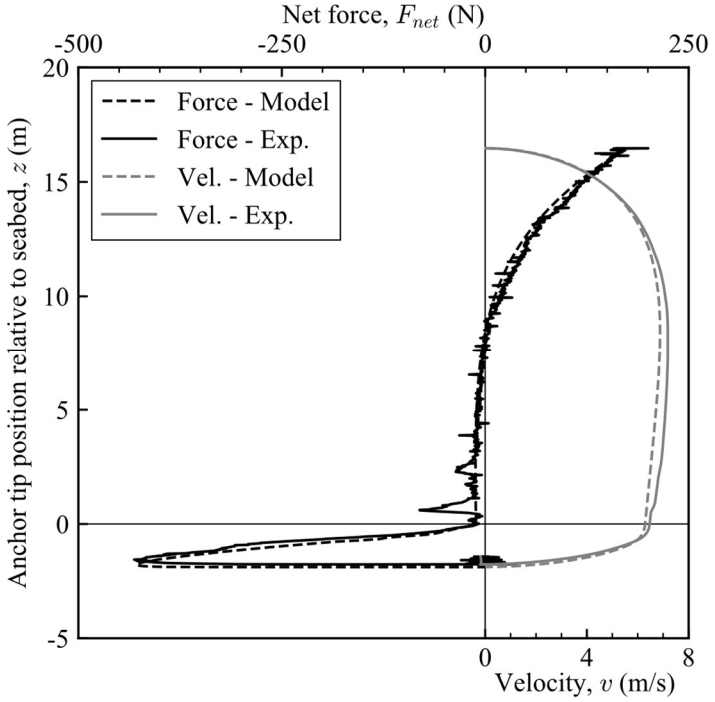

Figure 4. Measured and simulated responses for a dynamically-embedded anchor experiment described by O'Beirne et al. (2017a) – Test HD1 therein.

3 Installed monotonic plate anchor capacity

Once a plate anchor has been installed (whether dynamically or statically), the available capacity is calculated by considering the bearing capacity after keying. To allow a simple analytical treatment, only pure vertical monotonic capacity is considered assuming the plate is keyed into a horizontal orientation and subjected to a vertical load:

$$V_{ult} = N_c s_{u-op} A_{plate} + W'_{plate} \tag{4}$$

where s_{u-op} is the operative undrained strength at the plate centroid, A_{plate} is the projected area of the plate, W'_{plate} is the submerged (effective) weight of the plate in soil and N_c is a bearing capacity factor, calculated by:

$$N_c = \min\left[(5.14 * 1.2) * \left(1 + 1.2\, tan^{-1}\left(\frac{z_{op}}{D_p}\right)\right), 14.5\right] \tag{5}$$

where z_{op} is the embedment depth of the plate centreline after keying. Eq. 5 is based on the experimental results summarised by O'Loughlin et al. (2017) and Blake et al. (2015a) and is a modified version of the relationship provided in DNV (2002). Although the plate and load orientations depend on project-specific mooring configurations, these assumptions are appropriate for a range of initial embedment conditions and consistent with design practice.

The loss of plate embedment that occurs during keying is calculated as:

$$\frac{\Delta z_{key}}{D_p} = \frac{z_{in} - z_{op}}{D_p} = \frac{0.144}{\left[\left(\frac{e}{D_p}\right)\left(\frac{t_p}{D_p}\right)^{0.2}\right]^{1.15}} \tag{6}$$

where Δz_{key} is the loss of embedment during keying, z_{in} is the initial embedment after plate installation, $z_{op} = z_{in} - \Delta z_{key}$ is the operative plate embedment for capacity assessment, e is the eccentricity of the anchor padeye from the centreline of the plate (taken as $0.45D_p$ following O'Loughlin et al. 2014) and t_p is the thickness of the plate. Eq. 6 was derived from a database of large deformation finite element simulations (Wang et al. 2011) for a 90° plate rotation from vertical to horizontal and has been shown by O'Loughlin et al. (2014) to match the measured loss of embedment during keying in centrifuge experiments.

4 Model sensitivity under idealised scenarios

This section explores the influence of soil parameter uncertainty on both the installation depth and the resulting capacity of a DEPLA. The soil strength profile is based on baseline values listed in Table 2. To allow for a practical comparison of anchors of different sizes, the drop height for installation is set to that required to achieve 90% of terminal velocity on impact. For the constant length to diameter ratio of $\frac{L_f}{D_f} = 12$, this height is approximately $46.3D_f$. The anchor geometry and other parameters are scaled by retaining the dimensionless ratios in Table 1, with the follower diameter, D_f, being the fundamental dimension from which others are scaled.

Table 2. Baseline values for soil properties used in parametric study.

Property	Undrained Shear Strength Gradient	Mudline Shear Strength Intercept	Soil Effective Unit Weight	Soil Sensitivity	Soil Strain Rate Parameter	Soil Reference Strain Rate
	k	s_{u0}	γ_s'	S_t	β	$(v/D)_{ref}$
	(kPa/m)	(kPa)	(kN/m^3)	(-)	(-)	(s^{-1})
Value	1.5	0 (2)	4	4	0.07	0.56(2)

Note: (1) s_{u0} = 0.1 kPa adopted in the simulations to avoid division by zero.
(2) Representative value for a 35.7 mm diameter piezocone penetrated at 20 mm/sec.

4.1 Effect of undrained shear strength gradient

Figure 5a shows the effect of changing k on DEPLAs of varying scale. Two aspects are considered: (a) the anchor efficiency, defined as a ratio of the monotonic (post-keying) capacity to the dry weight of the plate V_{ult}/W_{plate}, and (b) the normalised as-installed embedment (prior to keying), z_{in}/D_p. The anchor scale, given by D_f, has minimal influence when the results are non-dimensionalised.

For all anchor sizes, there is a similar non-linear influence of strength gradient on embedment depth and anchor capacity. Lower soil strengths provide less resistance to decelerate the anchor,

increasing the embedment. However, the net effect is a reduction in the resulting plate capacity (although the trend reverses for $k \gtrsim 3$ kPa/m due to reductions in N_c at shallow depth – Eq. 5). The relationship between k and V_{ult}/W_{plate} is non-linear because the loss in capacity due to lower strength is partially compensated (or 'corrected') by increased embedment. This contrasts with a statically-embedded plate anchor that is embedded to a prescribed depth with capacity scaling linearly with k.

The self-correcting effect is highlighted on Figure 5b by comparing a DEPLA (D_f = 1.0 m; D_p = 4.8 m) with the equivalent circular plate (D_p = 4.8 m) statically-embedded to a specified depth. This example compares a plate statically-embedded to the same depth predicted for a DEPLA with an expected undrained strength gradient of $k_{exp} = 2$ kPa/m (i.e., z_{in}/D_p = 4.1). If the actual strength gradient, k_{act}, encountered is equal to k_{exp}, both the DEPLA and the statically-embedded plate have the same capacity. However, if $k_{act} < k_{exp}$ both the DEPLA (V_{DEPLA}) and statically-embedded (V_{static}) capacities will be less than expected. The reduced efficiency for the V_{DEPLA} in Figure 5b varies non-linearly with k because embedment also varies with k. Conversely, the statically-embedded capacity (dashed black line in Figure 5b) varies linearly with k because the embedment does not change but the operative undrained strength does. Hence, if the encountered soil is weaker than expected, the DEPLA reduces less in capacity (relative to the design value) than a statically-embedded equivalent.

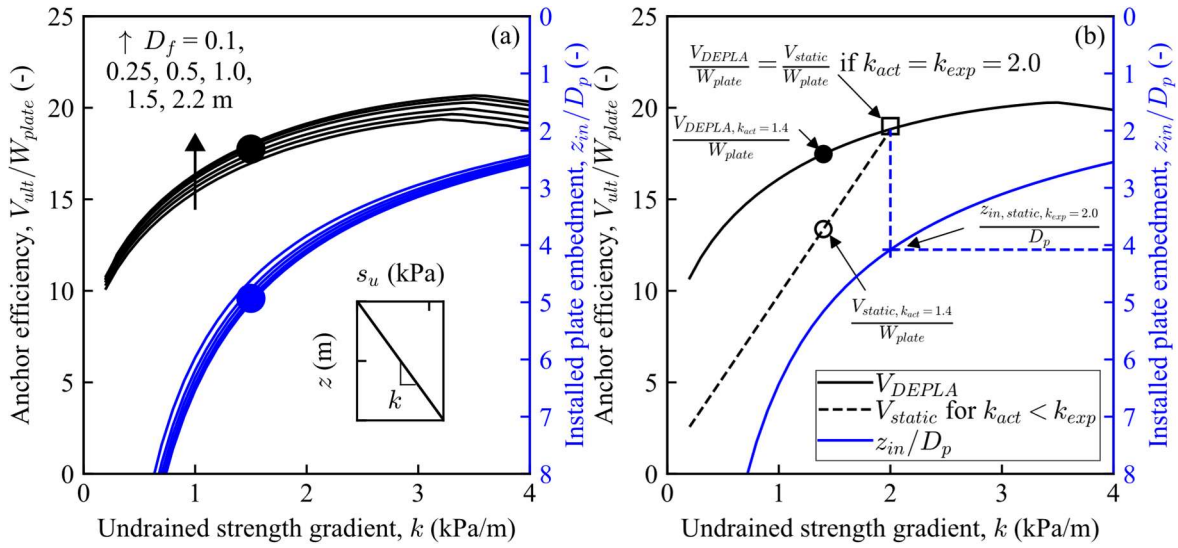

(a) (b)

Figure 5. Variation in anchor efficiency and installed (unkeyed) embedment with undrained shear strength gradient: (a) DEPLAs of varying D_f, solid circles represent baseline results for comparison with Figure 6; (b) comparing DEPLA with D_f = 1.0 m and the same sized circular plate statically embedded. Dashed lines represent variation in V_{static} for different k encountered, if statically embedded to DEPLA z_{in} based on expected k = 1, 2 and 3 kPa/m.

4.2 Effect of other soil parameters, s_{u0}, γ', S_t, β

This section considers the effects of the other soil parameters, s_{u0}, γ', S_t and β by independently varying each parameter relative to the baseline case with all others kept constant. These results are shown on Figure 6.

As s_{u0} increases, the smaller D_f cases ($D_f = 0.1, 0.25$ m) do not have enough impact energy to penetrate and the plate embedment after keying is less than $0.5D_p$. However, if the plate is embedded after keying, the anchor efficiency varies by less than 10% due to the modelled range of s_{u0}. This means that if an anchor can penetrate fully, it is primarily k, not s_{u0}, that controls anchor efficiency. Figure 6b shows the results are also insensitive to γ_s'. In contrast, increasing S_t causes a non-linear increase in embedment and in turn an increase in anchor capacity. A conservative design for dynamically-embedded anchors would consider smaller values of S_t.

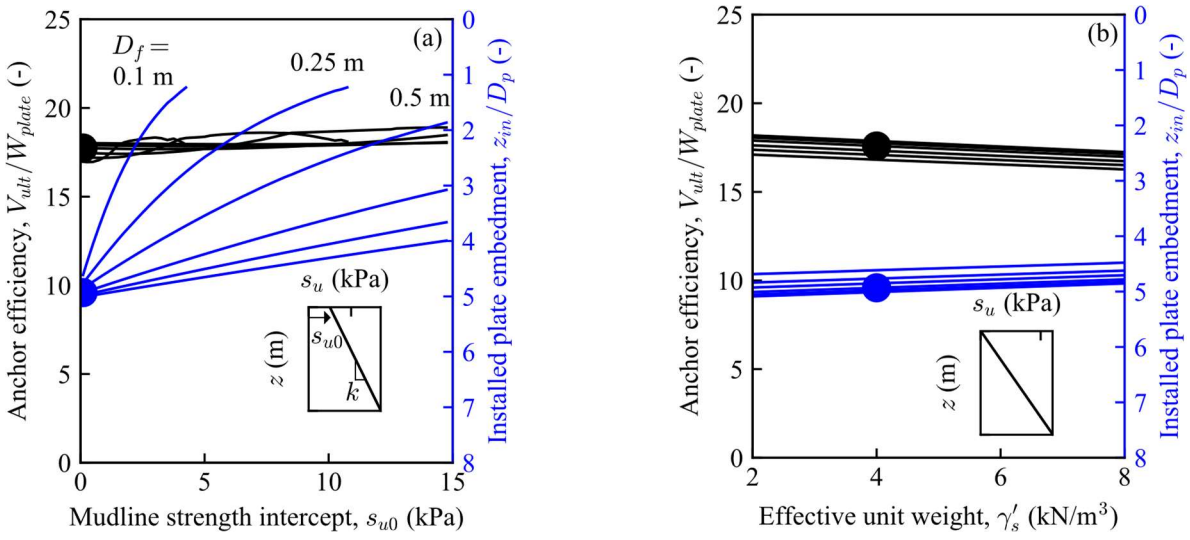

(a) (b)

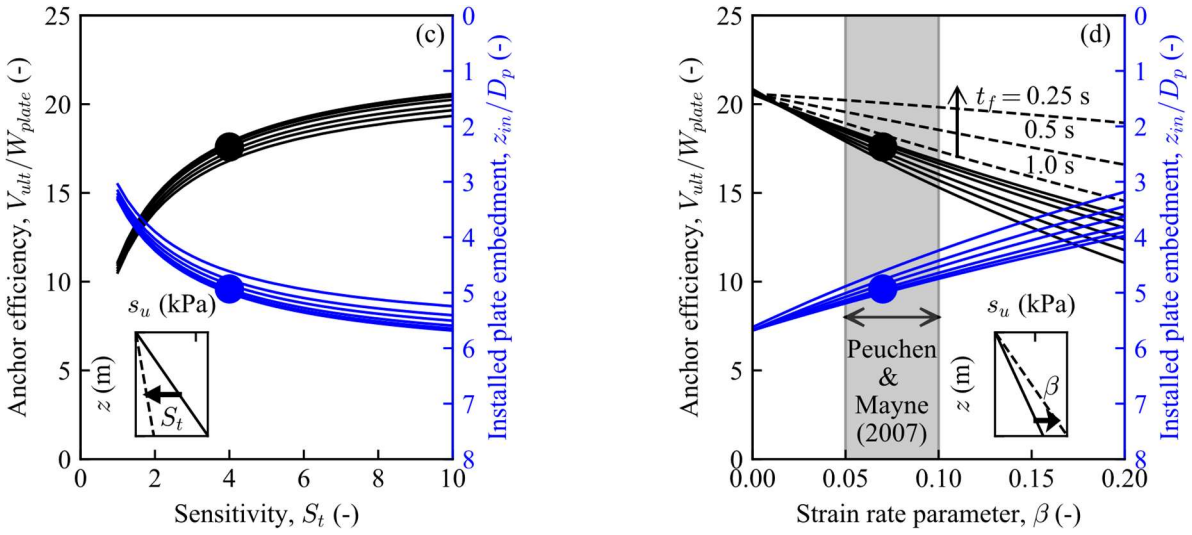

(c) (d)

Figure 6. Variation in anchor efficiency and installed (unkeyed) embedment with undrained shear strength gradient for: (a) s_{u0}, (b) γ', (c) S_t and (d) β. (d) also includes results for strain-rate enhanced monotonic capacity for different failure times, t_f, with D_f= 1.0 m. Solid circles represent baseline results for comparison with Figure 5.

The results for soil strain rate parameter (β) in Figure 6d show a direct relationship with reducing installation from the increasing effects of high anchor velocity and soil strain rate on the resistance during installation. However, if the range of potential values of β is within the indicated range reported by Peuchen & Mayne (2007), the variation is only around 10%.

These results assume that the ultimate capacity is the operative undrained strength measured directly from in situ testing. In other words, the undrained strength at failure is close to the same strain rate as the in situ test used to determine that strength (for instance 0.56 s^{-1} in the case of a standard cone penetrometer test). This assumption is consistent with design practice (e.g. see O'Loughlin et al. 2017); but if failure were to occur at faster rates due to snatch loads (e.g. see Hann et al. 2015), the resulting sensitivity to β is lessened because installation resistance and capacity are mobilised at comparable strain rates. Additional results plotted as dotted lines on Figure 6d illustrate this effect. For loading rates relevant for wave-loaded mooring systems, the failure period is on the order of 0.25 s because extreme snatch loads have shorter periods than the waves themselves (Hann et al. 2015; Lind et al. 2016). Hence, the variation in capacity resulting

from dynamic embedment for different β is reduced with the comparable strain rates during installation and loading. Plate anchors such as the DEPLA provide significant additional capacity from added mass effects during this type of rapid loading (Kwa et al. 2020).

5 Methodology for probabilistic uncertainty modelling

This section considers uncertainties associated with various governing parameters within a probabilistic framework. Probability distributions are assigned to the soil strength and the extreme anchor load, and Monte Carlo analyses are performed to assess the probability of failure and implied anchor reliability.

5.1 Probabilistic design approach: Monte Carlo method

DNV (2002; 2010) indicates that reliability-based design approaches, such Monte Carlo methods, may be used to demonstrate that the targeted annual probability of failure, $p_f = 10^{-4}$ (for ULS/Class 1) is achieved. Simple Monte Carlo methods work by running repeated calculations for a problem where the calculation inputs are selected as random variables from assumed probabilistic distributions. Each realisation corresponds to a combination of independent variables that are randomly drawn from their respective distributions, resulting in an output case. The outputs here are the installed embedment and anchor capacity for each realisation. Separately, the annual maximum load for that realisation is selected from a design load distribution as an additional independent random variable. In the Monte Carlo analysis, all partial factors are set to 1.0. For each realisation, the resulting system is classified as either safe or failed, where failure occurs if:

$$T_{d,i} > R_i \tag{7}$$

where $T_{d,i}$ is the design load for an individual realisation and R_i is the calculated capacity of that anchor realisation.

By conducting a sufficiently large number of realisations, probability distributions of the likelihood of the maximum annual design load exceeding the capacity are generated, from which the annual probability of failure is calculated as the probability that the load will exceed the capacity:

$$p_f = P\left(T_{d,i} > R_i\right) = \frac{\sum_{i=1}^{N}\left[T_{d,i} > R_i\right]}{N} \quad (8)$$

where N is the total number of realisations and [...] are Iverson brackets representing 1 if true and 0 if false. Another way to express Eq. 8 is in terms of a return period for failure, $RP_f = 1/p_f$.

5.2 Probabilistic inputs

5.2.1 Design loads

The distribution of mooring loads is based on the Stanisic et al. (2018) study of a large, permanently moored, weathervaning vessel with catenary moorings in metocean conditions relevant for offshore areas with significant tropical cyclone, typhoon or hurricane activity. The Stanisic et al. (2018) study was originally based on the specific conditions off the northwest coast of Western Australia. Stanisic et al. (2018) derived distributions of T_{MPM}, as the annual most probable maximum (peak) load at the anchor.

Stanisic et al. (2018) used the peak distribution method to establish the distribution of T_{MPM} based on metocean inputs for 100 yr and 10,000 yr return period events. The analyses assumed a water depth of 580 m with catenary moorings and a turret moored floating vessel. In this work, we use their results directly to represent expected anchor loads. Although values of T_{MPM} are strictly relevant for the assumptions and location considered, we apply the results to two sets of relevant soil conditions representing different regions to illustrate how reliability changes for different soil characteristics and levels of variability.

Figure 7a shows the distribution of T_{MPM} with respect to return period. For a 100 year return period event, the maximum line tension is approximately 8 MN; while a 1,000 year return period event is approximately 12 MN. The probability of non-exceedance for maximum tension (Figure 7b) represents the annual probability that the anchor will not experience a higher load during a given year. The line tension is assumed to be transmitted directly to the anchor itself so seabed friction and the mooring chain inverse catenary within the seabed are ignored. These assumptions are probably reasonable in extreme events as the catenary could be lifted from the seafloor, negating any seabed friction of the 'on-bottom' mooring chain.

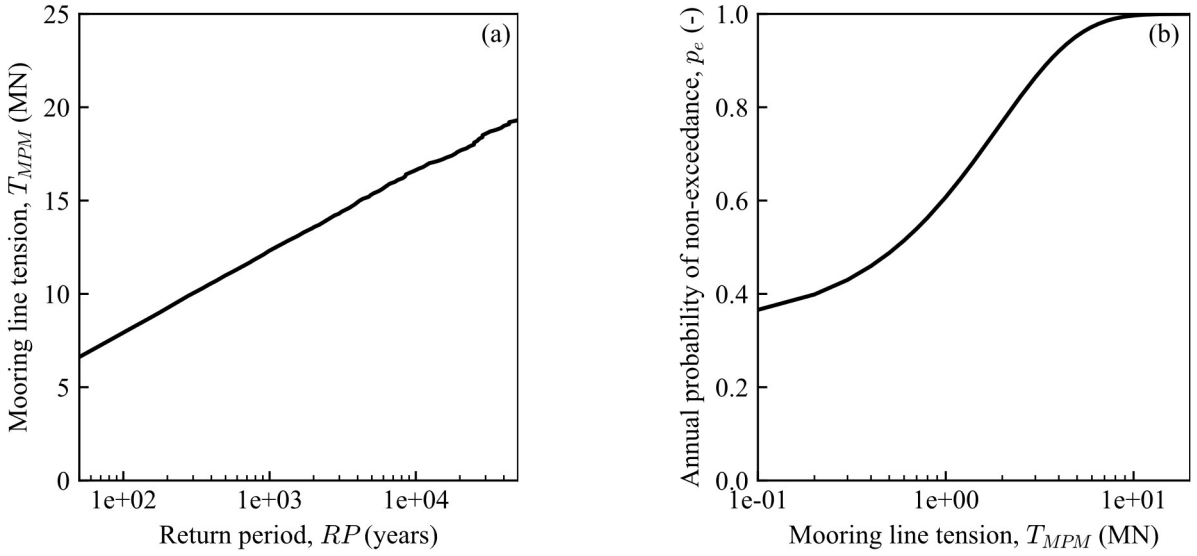

Figure 7. T_{MPM} probabilistic inputs: (a) variation with return period (RP); (b) cumulative distribution function of the annual probability of non-exceedance for different values of T_{MPM}.

5.2.2 Soil parameters

For the probabilistic assessment, we consider variations in the seabed strength profile representative of two geographical regions – the north west shelf of Australia (NWS) and the Gulf of Mexico (GoM). These represent different global regions where dynamically embedded anchors might be utilised. Importantly, the uncertainty in soil profiles for the two regions represent different types of strength variability. The variability for NWS conditions is primarily controlled by the mudline strength intercept, s_{u0} (Stanisic et al., 2019). The GoM features lower strength variability that is more dominated by variations in strength gradient, k (Cheon, 2010). Comparison using the same loading distribution illustrates the sensitivity to different soil characteristics. Table 3 summarises the distributions of soil parameters used for each site.

For NWS conditions, we use the 'high natural variability' case from Stanisic et al. (2019), with the parameters in Table 3. The mudline strength intercept is selected using the same random seed as k. Since a normal distribution is adopted, negative $s_{u,0}$ values are capped to a minimum of 0, which applies to approximately 10% of cases.

Table 3. Descriptive statistics for the probabilistic soil properties adopted for each site.

Property	Undrained Shear	Mudline Shear	Soil Effective	Soil	Soil Strain Rate	Soil Reference

	Strength Gradient	Strength Intercept	Unit Weight	Sensitivity	Parameter	Strain Rate
	k	s_{u0}	γ_s'	S_t	β	$(v/D)_{ref}$
	(kPa/m)	(kPa)	(kN/m^3)	(-)	(-)	(s^{-1})
NWS						
Distribution	Lognormal	Normal[1]	Normal	Normal	Uniform	Constant
Arithmetic Mean	1.73	10.25	4.0	3.33	0.075	0.56
Standard Deviation	0.118	6.54	0.5	0.50	0.014	
GoM						
Distribution	Lognormal	Lognormal[2]	Normal	Normal	Uniform	Constant
Arithmetic Mean	1.34	1.91	3.14	3.00	0.075	0.56
Standard Deviation	0.271	0.38	0.50	0.375	0.014	

Note: (1) For NWS, the same random variable was used for s_{u0} as used for k. A lower limit for s_{u0} = 0 kPa was adopted.
(2) For GoM, the same random variable was used for s_{u0} and k.

For GoM conditions, lognormal probabilistic distribution parameters for s_{u0} and k have been selected to approximately fit a database of undrained strength measurements compiled from 15 project sites in the GoM (Cheon, 2010). For GoM, the same random seed is used for k and s_{u0} reflecting the correlation between these parameters.

The adopted distributions for k and s_{u0} are shown on Figure 8 as cumulative distributions along with representative data from Stanisic et al. (2019) and Cheon (2010). From these strength parameters, a strength profile can be calculated for each site. The resulting strength profiles, in terms of 10th, 50th and 90th percentiles (i.e. P_{10}, P_{50} and P_{90}) are shown on Figure 9a. The range of strength profile is typical for fine-grained sediments offshore Western Australia (e.g., Erbrich and Hefer, 2002) and in the Gulf of Mexico (Cheon, 2010). The ratio, P_{90}/P_{10}, for the GoM is relatively

constant with depth (approximately 1.7), whereas P_{90}/P_{10} for the NWS site is higher and decreases with depth (e.g., 3.2 at z = 5 m and 1.9 at z = 5 m).

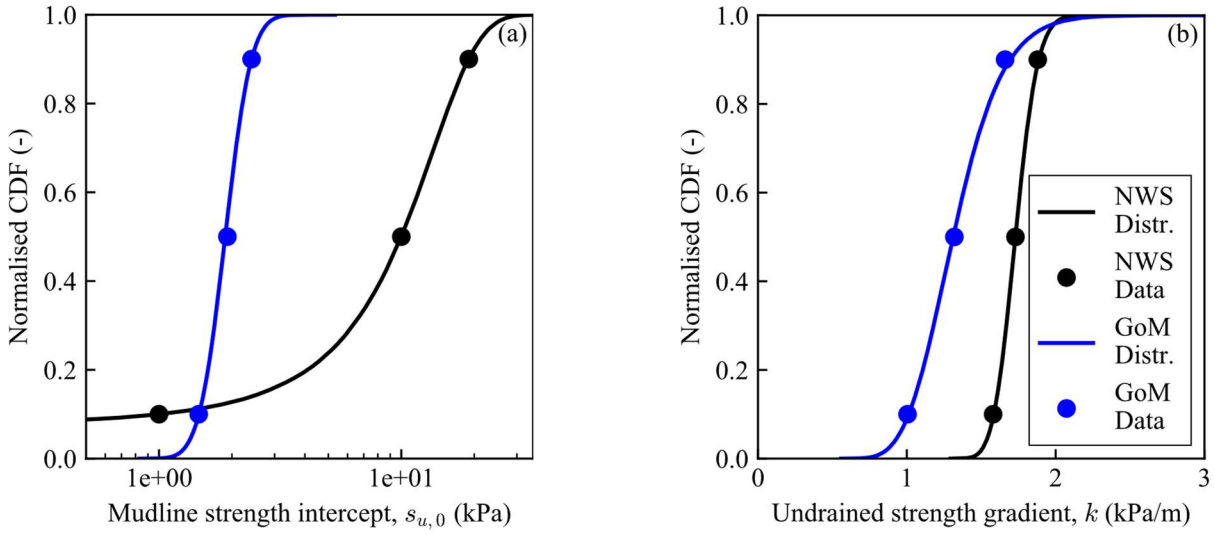

(a) Mudline undrained strength (b) Undrained strength gradient

Figure 8. Undrained strength gradient property probabilistic distributions for representative Northwest Shelf (NWS) and Gulf of Mexico (GoM) profiles. Data fitted from Stanisic et al. (2019) and Cheon (2010).

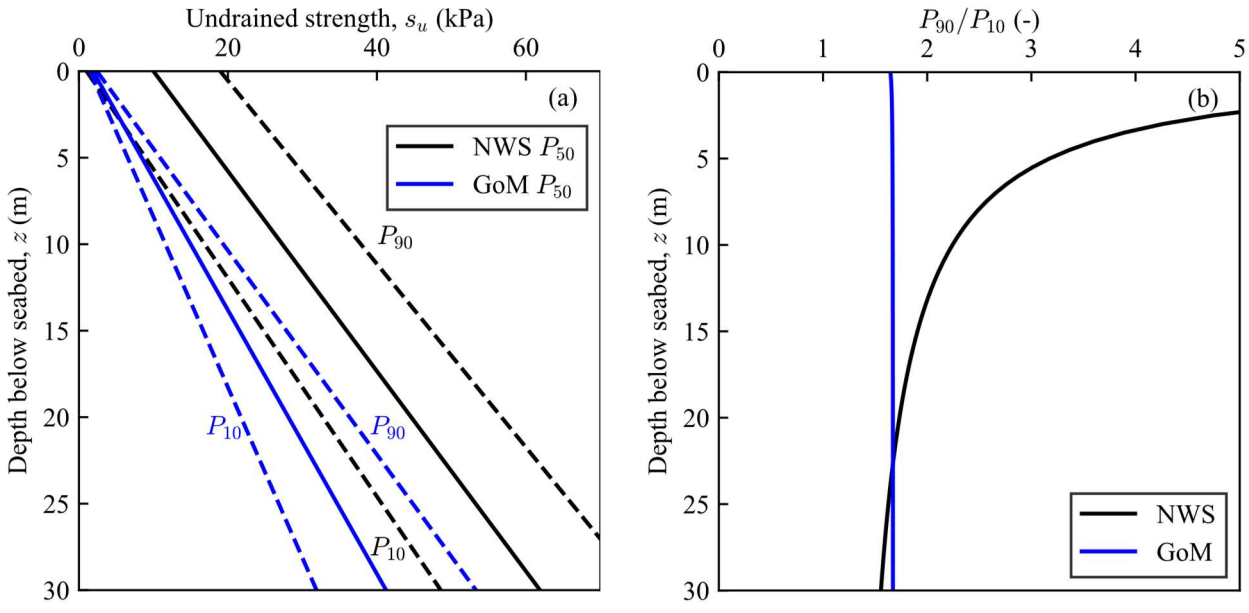

Figure 9. Characteristic strength profiles for the Northwest Shelf and Gulf of Mexico sites based

342 on adopted probabilistic distributions: (a) strength profile percentiles; (b) P_{90}/P_{10} ratios.
343

344 The remaining two soil properties that are considered probabilistically are the soil effective unit
345 weight, γ', and the soil sensitivity, S_t. The effective unit weights at both sites are represented by
346 normal distributions with μ = 4.0 kN/m^3 for NWS and μ = 3.14 kN/m^3 for GoM, with σ = 0.5
347 kN/m^3 for both sites. For the soil sensitivity, normal distributions are adopted with [μ, σ] of [3.33,
348 0.5] for NWS and [3.0, 0.375] for GoM. The distributions for NWS have been selected based on
349 Erbrich & Hefer (2002). The mean value of sensitivity for NWS (3.33) is representative of the
350 fine-grained sediments offshore Western Australia typically found in deeper waters (> 200 m).
351 The adopted distribution is hence lower than the much higher sensitivity values that are typical of
352 shallower-water coarser grained sandy silts and silty sands (e.g., Watson et al., 2019). GoM
353 distributions were selected from the remoulded strength measurements reported by Cheon (2010)
354 in conjunction with the intact undrained strength distributions described earlier. Figure 10 shows
355 the resulting cumulative distributions.

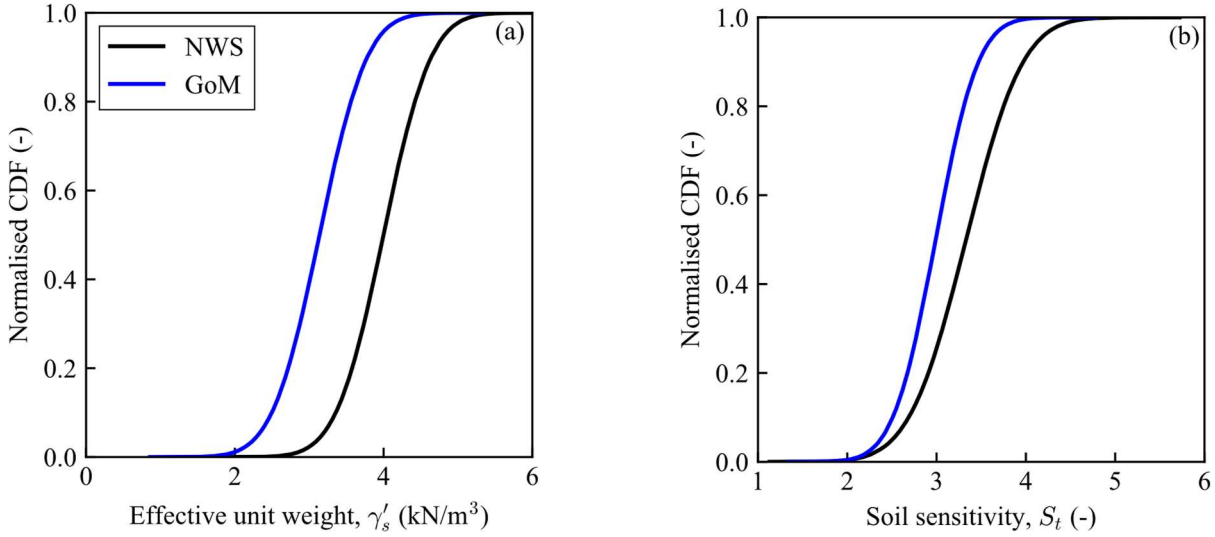

356

357 Figure 10. Cumulative distribution functions for: (a) unit weight and (b) soil sensitivity for
358 representative Northwest Shelf (NWS) and Gulf of Mexico (GoM) profiles.
359

360 Peuchen & Mayne (2007), reviewing data from in situ vane shear tests (some originally
361 compiled by Biscontin & Pestana 1999), suggested a range of $\beta = 0.075 \pm 0.025$ captures the
362 response for several onshore and offshore soils. This range is also consistent with back-analysis of

free-fall penetrometers (e.g., O'Loughlin et al. 2014; Blake and O'Loughlin 2015; O'Loughlin et al. 2016; O'Beirne et al. 2017b). A uniform distribution of β varying between 0.05 and 0.10 (i.e., following Peuchen & Mayne, 2007) has been adopted in the probabilistic assessments.

5.2.3 DEPLA dimension ranges

To compare a DEPLA with a statically-embedded circular plate, we consider a range of DEPLAs varying the follower diameter, D_f. The assumptions keep the ratio of follower length to diameter constant at 12:1, the ratio of fluke (plate) diameter to follower length constant at 0.4:1 and the ratio of fluke thickness to diameter constant at 0.05:1 (see Table 1). These ratios are adopted based on Blake and O'Loughlin (2015), and we adopt constant ratio scaling rules to ensure consistency for comparison between different anchor length scales. The total anchor density represents the overall density applied to the total volume of the DEPLA to calculate a given anchor mass. This is assumed constant at a value of 6000 kg/m^3, which allows for partially solid steel DEPLAs. The total weight of the anchor and the size of the embedded plate is varied by adjusting the plate diameter in the range D_p = 6.0 to 6.5 m. The drop height for installation is set to that required to achieve 90% of terminal velocity on impact, and the water depth is assumed to be greater than this drop height.

5.3 Monte Carlo analysis: required realisations

A sensitivity check was conducted to find the required number of Monte Carlo realisations to accurately capture the tails of the output distribution and the annual probability of failure. This check used ρ_a = 6000 kg/m^3, D_f = 1.4 m, the NWS site soil conditions and the load distribution with the magnitude increased to achieve an annual probability of failure, $p_f \approx 1e^{-4}$. The results are shown on Figure 11 in terms of the 10th, 50th and 90th percentile capacities and annual probabilities of failure. Above 10^4 realisations, there is negligible change in these percentile capacities. Figure 11b indicates a stable p_f is observed after ~10^5 realisations. To balance accuracy with reasonable computational needs, the results in the remainder of the paper use 2×10^5 realisations.

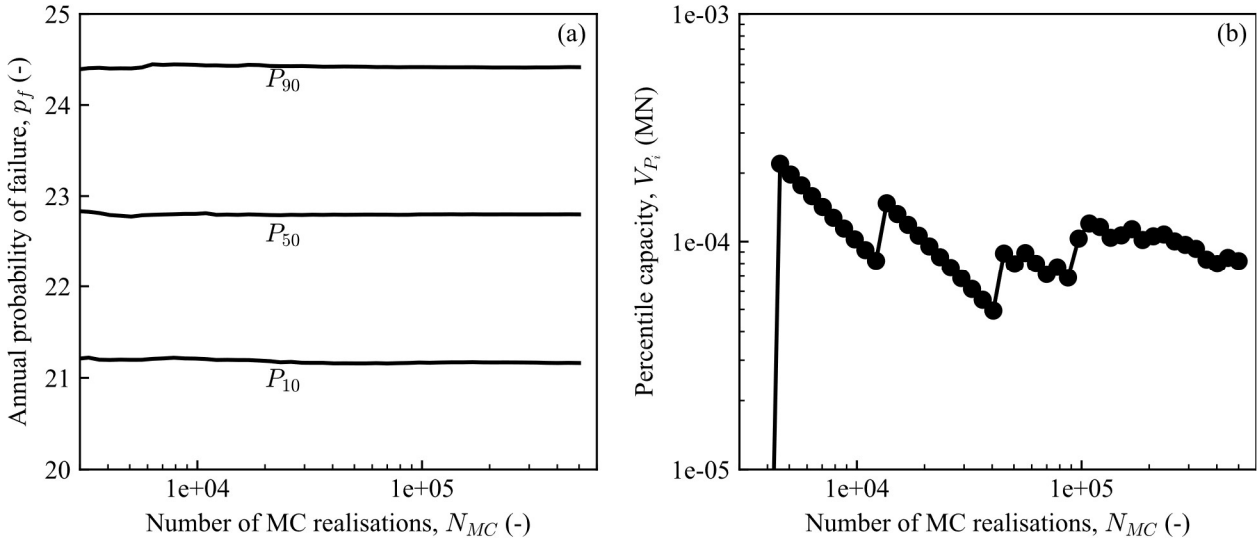

Figure 11. Dependency of Monte Carlo results on number of probabilistic runs: (a) percentile calculated capacity; (b) annual probability of exceedance.

6 Deterministic design of statically-embedded plate anchors

This section presents the deterministic design of a statically-embedded plate anchor using an LRFD (load and resistance factor design) approach with industry-standard partial factors for load and resistance. These calculations establish the required anchor dimensions. In Section 7, we use these results with a probabilistic approach to compare the reliability of a statically-embedded plate with an equivalent DEPLA, and the potential 'self-correction' for the DEPLA.

The deterministic design for a statically-embedded plate anchor follows a standard partial factor approach (e.g., DNV 2002; ISO 2013) as set out below:

1. The design undrained strength profile is the mean profile (Table 3).
2. The design load T_d is the annual maximum load on the anchor using the most probable maximum 100-yr load value (in this case 8.07 MN – Figure 7) and applying a partial load factor, γ_L = 1.65, such that $T_d = 13.3$ MN.
3. For a given plate diameter, the installed depth z_{in} at which the anchor capacity V_{ult} satisfies the required partial resistance factor ($\gamma_{res} = \frac{V_{ult}}{V_{design}} \geq 1.4$, so $V_{ult} = 18.6\ MN$), is calculated, including an allowance for additional depth requirements for keying embedment loss (Eqs. 4-6).

A partial resistance factor, γ_{res} = 1.4 is satisfied by a plate diameter, D_p = 6.5 m at a depth, z_{in} = 20.4 m for NWS soils, and at z_{in} = 31.3 m for GoM soils.

7 Probabilistic analysis of actual reliability

This section estimates the probability of failure associated with the LRFD-designed statically-embedded anchor and an equivalent DEPLA. The aim of this analysis is to (i) assess the reliability achieved by the recommended LRFD partial factors under the assumed conditions and (ii) quantify any 'self-correction' effect that arises from the dynamic embedment of the DEPLA.

7.1 Capacity distributions

Figure 12 shows the Monte Carlo distributions of capacity and embedment for different plate diameters for the NWS and GoM soil characteristics. All results are for $\rho_a = 6{,}000$ kg/m^3 and only D_p is varied. Monte Carlo capacity distributions for the statically-embedded anchors are also shown for the single case of D_p = 6.5 m.

The first trend evident in Figure 12 is that increases in plate diameter, D_p, give significant increases in DEPLA capacity. This is primarily due to the increased bearing area, which increases with the square of D_p for a given embedment depth, and to the deeper embedment from the larger anchor mass. The increase in penetration resistance during installation from the larger plate projected area is eclipsed by the increase in anchor weight (also demonstrated by O'Loughlin et al. 2013). Although the relationship between D_p and z_{in} is non-linear due to non-linearities in the anchor embedment model, the dependence of V_{ult} on z_{in} is approximately linear as s_u increases linearly with depth in these calculations.

The second observation from Figure 12 is that the DEPLA capacity has a narrower distribution than the statically-embedded equivalent. This is due to the 'self-correcting' nature of the DEPLA. By contrast, statically-embedded anchors with a fixed embedment depth result in a capacity distribution that is directly related to the soil strength distribution.

Finally, there is a wider distribution of DEPLA plate embedment for the NWS site than the GoM. This increased variation is caused by the adopted distribution for s_{u0} (and the 0 kPa cut-off), which causes a larger ratio of P_{90}/P_{10} strength at shallower depths, creating a larger range of embedments at the shallow tail (Figure 9). In contrast, the ratio of P_{90}/P_{10} strength is approximately

436 constant with depth for the GoM soils as each strength profile approaches s_{u0} = 0 kPa linearly as
437 depth reduces. The asymmetrical DEPLA embedment distribution for the NWS site is an effect of
438 the strength distribution.

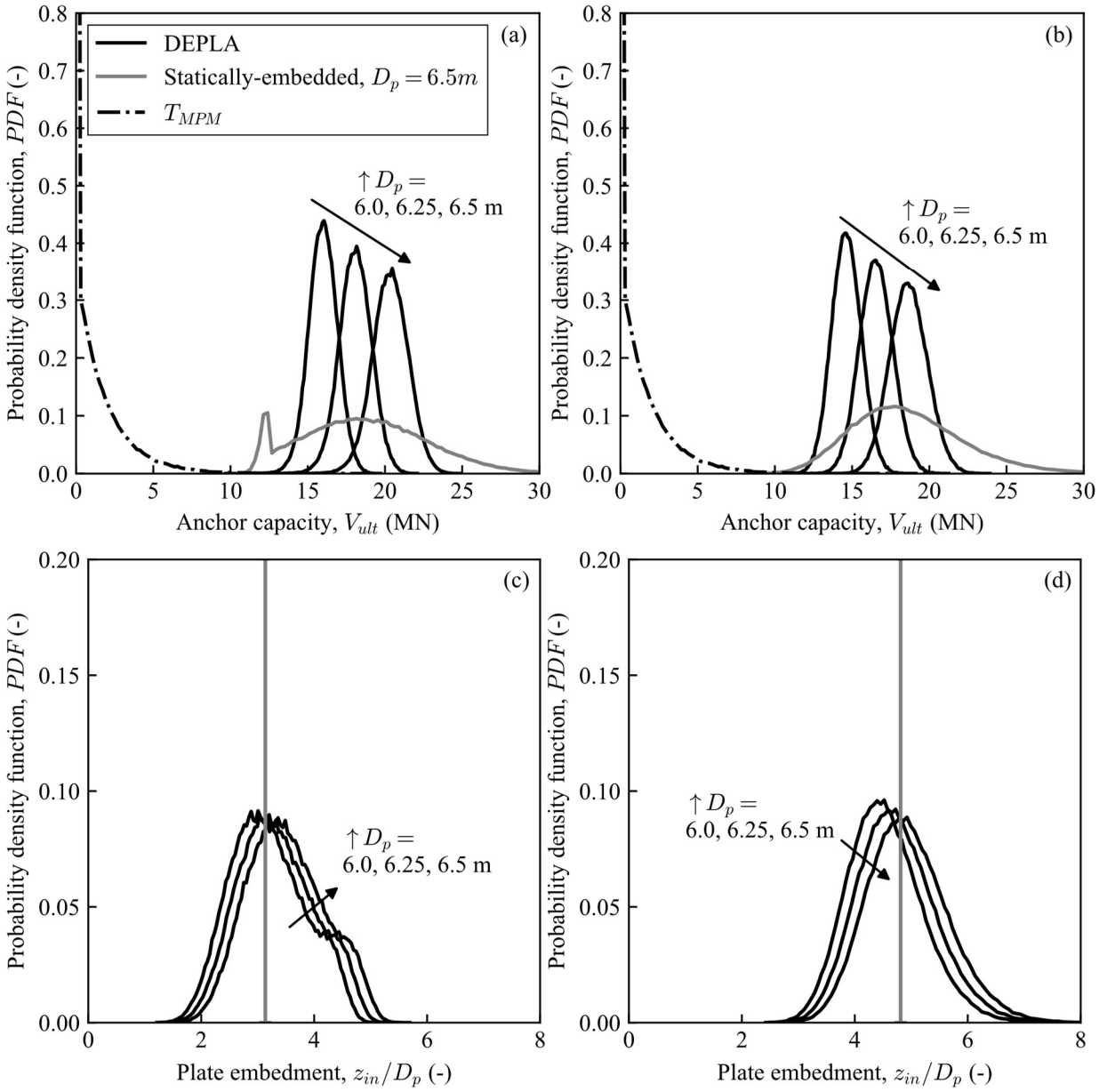

439
440

441 Figure 12. Distribution of capacities and embedments for the NWS (a, c) and GoM (b, d) site
442 conditions for the DEPLA and the statically-embedded equivalent anchor: (a, b) anchor capacity,
443 (c, d) plate embedment.

444

7.2 Required partial resistance factors and probability of failure

This section compares the reliability of DEPLAs compared to the equivalent statically-embedded plate anchor, and quantifies the applicable design partial resistance factor for the DEPLA to achieve the same reliability. This is done by calculating the annual probability of failure, p_f, from capacity distributions for a range of DEPLA sizes, combined with the annual maximum load T_{MPM} (Figure 12).

Figure 13 compares p_f results calculated by Equation 8 for both DEPLA and statically-embedded plates for different values of partial resistance factor:

$$\gamma_{res} = \bar{V}_{ult}/T_d \quad (9)$$

where $\bar{V}_{ult}$ is the ultimate monotonic capacity (Section 3) calculated using the mean of the adopted soil strength distributions and T_d is the design tension load as per Section 5.2.1. The statically-embedded plate results on Figure 13 plot at γ_{res} = 1.4 (recalling that this was the design basis from Section 6), with $p_f = 1.55 \times 10^{-4}$ for the NWS site and $p_f = 1.10 \times 10^{-4}$ for the GoM site, established from the 200,000 Monte Carlo realisations. The DEPLA results (for the same plate diameter, D_p = 6.5 m) on Figure 13 achieved a lower probability of failure for both site conditions $p_f = 1.0 \times 10^{-5}$ for the NWS site conditions and $p_f = 2.5 \times 10^{-5}$ for the GoM site conditions. However, these lower probabilities of failure are associated with larger partial resistance factors, calculated via Eq. 9 using soil properties that are the mean values of the assumed distributions (Section 5.2.2) of γ_{res} = 1.53 for NWS and γ_{res} = 1.41 for GoM.

Figure 13 also shows additional results for the DEPLA where the overall anchor scale (and hence D_p) was progressively reduced, with a corresponding reduction in partial resistance factor, γ_{res}. The results for both sites fall along a similar exponential line given by:

$$p_f = \exp(1.61 - 8.58 * \gamma_{res}) \quad (10)$$

These additional results demonstrate that similar p_f can be achieved with smaller DEPLA plates relative to that needed for a static embedment – D_p ~ 6.0 m (NWS) and 6.25 m (GoM), compared to D_p = 6.5 m for the statically-embedded case. Moreover, the partial resistance factor for the DEPLA to achieve the same reliability as the equivalent statically-embedded plate anchor reduces to γ_{res} = 1.21 (NWS) and 1.25 (GoM) using the fitted exponential relationship shown on Figure

471 13. This outcome is consistent with the narrower spreads in the DEPLA Monte Carlo results
472 illustrated on Figure 12, and therefore the reduced overlap between load and resistance.

473

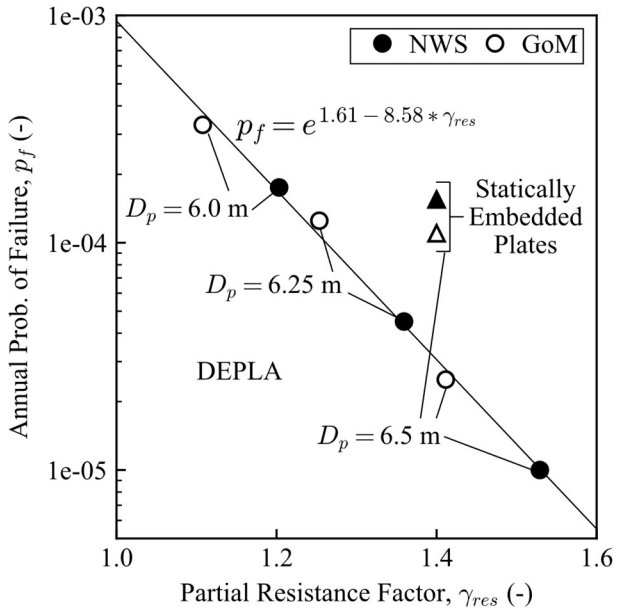

474

475 Figure 13. Comparison of calculated partial resistance factor (Eq. 9) with annual probability of
476 failure NWS and GoM soil conditions. Exponential best fit to the DEPLA results is also shown.

477

478 From these results, anchor selection for these example conditions can be based on Eq. 9 by
479 selecting values of γ_{res} corresponding to the required reliability to be achieved by the DEPLA. In
480 addition to quantifying the higher reliability of the DEPLA, this type of insight from the Monte
481 Carlo analysis is useful if reliability-based or risk-informed design is adopted (e.g. under ISO
482 2015). These design approaches allow the adopted p_f to be tailored to the associated risk, which
483 depends on whether the structure is crewed or uncrewed, the risk of environmental impact, the
484 business impact of failure, as well as other factors.

485 For both the NWS and GoM soils, the targeted reliability of $p_f = 10^{-4}$ recommended by DNV
486 (2002), at least for the conditions considered herein, is achieved with $\gamma_{res} \approx 1.25$ for the DEPLA.
487 In practical terms, the required γ_{res} sets the targeted value of $\bar{V}_{ult}$ that must be achieved using the
488 mean soil properties at a given site. Iteration is then required in which the DEPLA scale is varied
489 until the required value of $\bar{V}_{ult}$ is achieved. The specific value of γ_{res} depends on the distributions

of soil properties and most probable maximum loads, although very similar γ_{res} trends were observed for both soil sites, with two different geotechnical uncertainty profiles. These findings are therefore likely to be typical for many floating systems in different metocean environments and seafloor conditions worldwide. Overall, the results demonstrate the potential benefits of dynamic installation in reducing the expected uncertainty in capacity (i.e., spread in capacity distribution), compared to statically-embedded equivalent systems.

8 Concluding remarks

This paper presents a series of parametric and probabilistic Monte Carlo simulations to explore uncertainty associated with dynamically-embedded anchors, specifically DEPLAs. Calculations were conducted using an explicit numerical approach to calculate the embedment, and monotonic capacity was assessed using standard bearing capacity methods.

Compared to equivalently-sized circular plate anchors statically embedded to a specified depth, the DEPLA demonstrates a 'self-correcting' nature. Encountering soil strength different from expectations has less detrimental impact on the achieved embedment and capacity of DEPLAs than statically-embedded equivalents. Weaker than expected soil will result in greater anchor embedment from dynamic installation, increasing the capacity relative to a statically-embedded anchor installed to the depth that was expected to be achieved by the DEPLA. Conversely, if the soils are stronger than expected, the DEPLA will not penetrate as far into the seabed; but the capacity will remain higher than expected in design.

Monte Carlo analyses were conducted for two soil profile characteristics for global locations (the Northwest Shelf of Australia and the Gulf of Mexico) but more importantly representative of different characteristics of undrained strength uncertainty. For the Northwest Shelf, the uncertainty is primarily associated with the mudline strength intercept; while for the Gulf of Mexico, the uncertainty is associated with the strength gradient. In both cases, probabilistic analyses demonstrate lower capacity uncertainty for the DEPLA compared to equivalently-sized, statically-embedded plate anchors designed using LRFD-type approaches. We present a preliminary design approach that might be utilised to design a DEPLA and demonstrate that smaller partial resistance factors may potentially be utilised for the DEPLA to achieve equivalent system reliabilities to an equivalent statically-embedded plate.

In summary, this paper demonstrates that dynamic installation can lead to higher reliability relative to static installation, which may be quantified via probabilistic analyses that allow reduced LRFD partial resistance factors to be calibrated. This study also shows that reliable estimation of the embedment depth for dynamically installed anchors may be less critical for a reliable design. Previous studies have described this as a significant design challenge and disadvantage of dynamically-embedded anchors, due to the complexity of dynamic penetration coupled with any uncertainty in the site strength profile. This study demonstrates that these uncertainties are reduced by the self-correcting behaviour, so have minimal influence on anchor capacity reliability.

9 Acknowledgements

This work was supported by the ARC Industrial Transformation Research Hub for Offshore Floating Facilities, which is funded by the Australian Research Council, Woodside Energy, Shell, Bureau Veritas and Lloyds Register (Grant No. IH140100012). The final author is also supported by the EPSRC Offshore Renewables Energy Supergen Hub (grant EP/Y016297/1).

10 References

Ackroyd, J. A. D. (1982). On the analysis of turbulent boundary layers on slender cylinders. *Journal of Fluids Engineering*, 104, 185-190.

Andersen, K. H., Murff, J. D., Randolph, M. F., Clukey, E. C., Erbrich, C. T., Jostad, H. P., ... & Supachawarote, C. (2005). Suction anchors for deepwater applications. In *Proceedings of the 1st International Symposium on Frontiers in Offshore Geotechnics, ISFOG, Perth* (pp. 3-30).

API (2005). Recommended Practice for Design and Analysis of Station Keeping Systems for Floating Structures, API RP-2SK. *American Petroleum Institute*, Washington.

Biscontin, G., & Pestana, J. M. (2001). Influence of peripheral velocity on vane shear strength of an artificial clay. *Geotechnical Testing Journal*, *24*(4), 423-429.

Blake, A. P., O'Loughlin, C. D., & Gaudin, C. (2015). Capacity of dynamically embedded plate anchors as assessed through field tests. *Canadian Geotechnical Journal*, *52*(1), 87-95.

Blake, A. P., & O'Loughlin, C. D. (2015). Installation of dynamically embedded plate anchors as assessed through field tests. *Canadian Geotechnical Journal*, *52*(9), 1270-1282.

Boylan, N. P., Roux, A., Colliat-Dangus, J. L., & Sato, A. (2017). Installation Response of 5.5 m Diameter Driven Piles in Carbonate Soil–The Ichthys Development. In *Offshore Site Investigation Geotechnics 8th International Conference Proceeding* (Vol. 674, No. 681, pp. 674-681). Society for Underwater Technology.

Cheon, J. Y. (2010). *Analysis of spatial variability in geotechnical data for offshore foundations* [Doctoral dissertation, University of Texas, Austin].

DNV – Det Norske Veritas (2002). Recommended Practice RP-E302: Design and installation of plate anchors in clay. *Norway: Det Norske Veritas*.

DNV – Det Norske Veritas (2010). Offshore Standard DNV-OS-E301: Position Mooring. *Norway: Det Norske Veritas*.

dos Santos, A. B., Henriques, C. C. D., & Pimenta, J. M. M. H. A. (2004). Improvements Achieved in the Project of FPSO P-50. In *Offshore Technology Conference*. Offshore Technology Conference.

Erbrich, C. T., & Neubecker, S. R. (1999). Geotechnical design of a grillage and berm anchor. In *Offshore Technology Conference*. Offshore Technology Conference.

Hann, M., Greaves, D. & Raby, A. (2015). Snatch loading of a single taut moored floating wave energy converter due to focussed wave groups. *Ocean Engng* 96, 258–271.

ISO (2013). Specific requirements for offshore structures − Part 7: Stationkeeping systems for floating offshore structures and mobile offshore units, ISO19901-7. *International Organization for Standardization*, Geneva.

ISO (2015) General principles on reliability for structures. ISO 2395:2015. *International Organization for Standardization*, Geneva.

Kwa K., Weymouth G., White D.J. & Martin C.M. (2021). Analysis of the added mass term in soil bearing capacity problems. *Geotechnique Letters*. 11(1):80-87. https://doi.org/10.1680/jgele.20.00097

Lind, S. J., Stansby, P. K. & Rogers, B. D. (2016). Fixed and moored bodies in steep and breaking waves using SPH with the Froude–Krylov approximation. *J. Ocean Engng Marine Energy* 2, No. 3, 331–354.

O'Beirne, C., O'Loughlin, C. D., & Gaudin, C. (2017a). A release-to-rest model for dynamically installed anchors. *Journal of Geotechnical and Geoenvironmental Engineering*, 143(9), 04017052.

O'Beirne, C., O'Loughlin, C. D., & Gaudin, C. (2017b). Assessing the penetration resistance acting on a dynamically installed anchor in normally consolidated and overconsolidated clay. *Canadian Geotechnical Journal*, 54(1), 1-17.

O'Loughlin, C. D., Randolph, M. F., & Richardson, M. (2004). Experimental and theoretical studies of deep penetrating anchors. In *Offshore Technology Conference*. Offshore Technology Conference.

O'Loughlin, C. D., Blake, A. P., Wang, D., Gaudin, C., & Randolph, M. F. (2013a). The dynamically embedded plate anchor: results from an experimental and numerical study. In *International Conference on Offshore Mechanics and Arctic Engineering* (Vol. 55409, p. V006T10A034). American Society of Mechanical Engineers.

O'Loughlin, C. D., Richardson, M. D., Randolph, M. F., & Gaudin, C. (2013b). Penetration of dynamically installed anchors in clay. *Géotechnique*, 63(11), 909-919.

O'Loughlin, C. D., Blake, A. P., Richardson, M. D., Randolph, M. F., & Gaudin, C. (2014). Installation and capacity of dynamically embedded plate anchors as assessed through centrifuge tests. *Ocean Engineering*, *88*, 204-213.

O'Loughlin C.D. White D.J. & Stanier S.A. (2015). Novel anchoring solutions for FLNG - Opportunities driven by scale. Proc. Offshore Technology Conference. Houston. OTC26032-MS

O'Loughlin, C. D., Blake, A. P., & Gaudin, C. (2016). Towards a simple design procedure for dynamically embedded plate anchors. *Géotechnique*, *66*(9), 741-753.

O'Loughlin, C. D., White, D. J., & Stanier, S. A. (2017). Plate anchors for mooring floating facilities–a view towards unlocking cost and risk benefits. In *Offshore Site Investigation Geotechnics 8th International Conference Proceeding* (Vol. 978, No. 986, pp. 978-986). Society for Underwater Technology.

Øye, I. (2000). Simulation of trajectories for a deep penetrating anchor. *CFD Norway Report*, *250*, 2000.

Peuchen, J., & Mayne, P. (2007). Rate effects in vane shear testing. In *Offshore Site Investigations and Geotechnics, Confronting New Challenges and Sharing Knowledge*. Society of Underwater Technology.

Stanisic, D., Efthymiou, M., Kimiaei, M., & Zhao, W. (2018). Design loads and long term distribution of mooring line response of a large weathervaning vessel in a tropical cyclone environment. *Marine Structures*, *61*, 361-380.

Stanisic, D., Efthymiou, M., White, D. J., & Kimiaei, M. (2019). Reliability of mooring lines and piles for a permanently manned vessel in a tropical cyclone environment. *Applied Ocean Research*, *82*, 430-446.

Raaj, S.K., Saha, N., & Sundaravadivelu, R. (2022). Freefall hydrodynamics of torpedo anchors through experimental and numerical analysis. *Ocean Engineering*, *243*, 110213.

Wang, D., Hu, Y., & Randolph, M. F. (2011). Keying of rectangular plate anchors in normally consolidated clays. *Journal of Geotechnical and Geoenvironmental Engineering*, *137*(12), 1244-1253.

Watson, P., Bransby, F., Delimi, Z. L., Erbrich, C., Finnie, I., Krisdani, H., Meecham, C., O'Neill, M., Randolph, M. F., Rattley, M., Silva, M., Stevens, B., Thomas, S., & Westgate, Z. (2019). Foundation design in offshore carbonate sediments–building on knowledge to address future challenges. In *From Research to Applied Geotechnics: Invited Lectures of the XVI Pan-American Conference on Soil Mechanics and Geotechnical Engineering (XVI PCSMGE), 17-20 November 2019, Cancun, Mexico* (Vol. 7, p. 240). IOS Press.

Wilde, B., Treu, H., & Fulton, T. (2001). Field testing of suction embedded plate anchors. In *The Eleventh International Offshore and Polar Engineering Conference*. International Society of Offshore and Polar Engineers.

Zhou, Z., O'Loughlin, C. D., White, D. J., & Stanier, S. A. (2020). Improvements in plate anchor capacity due to cyclic and maintained loads combined with consolidation. *Géotechnique*, *70*(8), 732-749.

Zimmerman, E. H., Smith, M., & Shelton, J. T. (2009). Efficient gravity installed anchor for deepwater mooring. In *Offshore Technology Conference*. Offshore Technology Conference.